General Disclaimer

One or more of the Following Statements may affect this Document

- This document has been reproduced from the best copy furnished by the organizational source. It is being released in the interest of making available as much information as possible.

- This document may contain data, which exceeds the sheet parameters. It was furnished in this condition by the organizational source and is the best copy available.

- This document may contain tone-on-tone or color graphs, charts and/or pictures, which have been reproduced in black and white.

- This document is paginated as submitted by the original source.

- Portions of this document are not fully legible due to the historical nature of some of the material. However, it is the best reproduction available from the original submission.

Produced by the NASA Center for Aerospace Information (CASI)

NASA Technical Memorandum 78531

Bi-Directional, Buried-Wire Skin-Friction Gage

Hiroshi Higuchi and David J. Peake

(NASA-TM-78531) BI-DIRECTIONAL, BURIED-WIRE SKIN-FRICTION GAGE (NASA) 27 p HC A03/MF A01 CSCL 20D

N79-14330

Unclas
G3/34 42059

November 1978

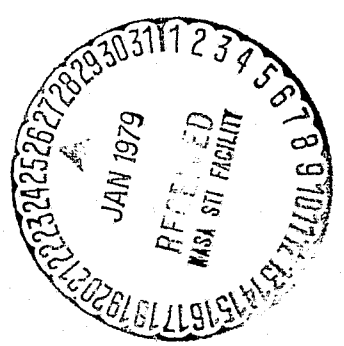

National Aeronautics and
Space Administration

SYMBOLS

A	calibration parameter (see eqs. (1) and (2))
B	calibration parameter (see eqs. (1) and (2))
d	overall diameter of a buried-wire, skin-friction gage (see fig. 1)
E	mean voltage drop across buried wire
g	amount of recess of probe installed on a curved surface
K	coefficient of directional sensitivity (see eq. (2))
M_∞	free-stream Mach number
R	electrical resistance
ΔR	difference between resistances of a wire at operating temperature, T_{wire}, and local wall temperature, T_{wall}
R_c	radius of curvature of model
S	electrical power term, defined in Equation (4)
T_0	reference temperature
T_{wall}	adiabatic wall temperature
T_{wire}	operating temperature of buried wire
ΔT	wire overheat temperature, $T_{wire} - T_{wall}$
α	angle between wall shear stress vector and a normal to buried wire (see eq. (2) and fig. 6)
α_0	temperature coefficient of resistance
α_c	angle of incidence of cone
θ	angle between wall shear stress vector and gage centerline bisecting the internal angle between individual buried wires (see fig. 1)
θ_c	cone semiangle
μ_w	viscosity of air at wall
ρ_w	density of air at wall
τ_w	mean wall shear stress

PRECEDING PAGE BLANK NOT FILMED

ϕ circumferential angle around cone surface, measured from windward generator

ω angle between tangent to limiting streamline (surface shear stress trajectory) and cone generator

Subscripts

A line of attachment or reattachment

C test model

S1 primary separation line

S2 secondary separation line

W or Wall } wall quantity

Wire buried-wire quantity

0 reference condition for temperature coefficient of resistance, see Section 4

1,2 sensor 1 and 2 on bi-directional, buried-wire gage (see fig. 1)

∞ free-stream mean condition

BI-DIRECTIONAL, BURIED-WIRE, SKIN-FRICTION GAGE

Hiroshi Higuchi

Dynamics Technology, Inc.*

and

David J. Peake

Ames Research Center

SUMMARY

A compact, nonobtrusive, bi-directional, skin-friction gage has been developed to measure the mean shear stress beneath a three-dimensional boundary layer. The gage works by measuring the heat flux from two orthogonal wires embedded in the surface. Such a gage was constructed and its characteristics were determined for different angles of yaw in a calibration experiment in subsonic flow with a Preston tube used as a standard. Sample gages were then used in a fully three-dimensional turbulent boundary layer on a circular cone at high relative incidence, where there were regimes of favorable and adverse pressure gradients and three-dimensional separation. Both the direction and magnitude of skin friction were then obtained on the cone surface.

INTRODUCTION

Ludwieg (ref. 1) was the first to introduce a skin-friction gage for measurements beneath a turbulent boundary layer, the principle of which depends on the heat transfer from the wall into the laminar sublayer. Liepmann and Skinner (ref. 2) established effects of pressure gradient and compressibility on gage performance and obtained a unique calibration in both laminar and turbulent flows. This type of heat-transfer gage is claimed to be less sensitive to pressure gradient (ref. 3) than other instruments such as a floating balance, a Preston tube, or a sublayer fence.

The directional sensitivity of a single-element heat-transfer gage was first demonstrated by Ludweig (ref. 1), and the measurement was repeated by Drinkuth and Pierce (ref. 4). McCroskey and Durbin (ref. 5) developed a double-sensor hot-film gage for three-dimensional boundary layers and calibrated the gage for its directional and magnitude sensitivity. In the construction of this gage, nickel is chemically deposited on a thin plastic film and, after the calibration, the gage can be bonded to a test surface. The overall size of the gage in planview is ~10 mm (~0.4 in.) and is appropriate for the large-scale wing and rotor blade models for which it was

---

*Dynamics Technology, Inc., Torrance, California 90503.

designed. The gage can be placed in any desired location, but in the current design, the gage and the connecting leads protrude into the boundary layer (i.e., the roughness height is large for its use in the high Reynolds number, turbulent boundary layers).

To accurately measure the convected heat transfer into the boundary layer, it is crucial that the conduction heat loss into the substrate of the gage is kept as low as possible. Most of the commercially available gages, with their sensors mounted on thick quartz rods, give unsatisfactory results in this respect. The conduction heat loss of the McCroskey gage (ref. 5) depends significantly on the type of surface to which the gage is attached. Rubesin et al. (ref. 6) tested various substrate materials and made a considerable improvement in reducing conduction heat loss by casting a wire into a thin layer of epoxy on a polystyrene substrate. Murthy and Rose (ref. 7) extended Rubesin's work and introduced a simplified fabrication process by applying solvent to "bury" a wire on the substrate.

The present investigators utilized the idea of the McCroskey gage and the fabrication technique of Murthy and Rose to develop a compact (3.18 mm (0.125 in.) overall diameter) bi-directional, buried-wire, skin-friction gage for measurements beneath three-dimensional, turbulent boundary layers. The construction and calibration of the gage and the representative results of the shear stress magnitude and direction on a circular cone model at incidence in a Mach 0.6 airstream are presented here.[1]

The gages tested here were fabricated by Fred Lemos in the Model and Instrument Machining Branch at Ames. His skillful efforts are hereby acknowledged.

GAGE FABRICATION

The present configuration of the skin-friction gage is shown in figure 1; its fabrication essentially followed the procedure for a single-element gage reported by Murthy and Rose (ref. 7). Four nickel electrodes were placed in a mold and polystyrene was injected to form a 3.18-mm (0.125-in.)-diameter plug around the electrodes. Tungsten wires, 5 μ in diameter, were then spot-welded to the exposed ends of the electrodes. A drop of ethyl acetate solvent was then applied to the exposed end of the gage using a miniature syringe. The solvent dissolves a thin layer of the polystyrene so that the tungsten wires become immersed and coated due to the capillary action of the liquid polystyrene, which eventually rehardens and "buries" the tungsten wires. The probe was protected from room drafts during this rehardening period to prevent rippling of the surface.

---

[1]While this report is concerned with the mean shear stress measurement, a further study is underway that concerns the gage sensitivities to the fluctuating shear stress, pressure, and flow direction.

It is appropriate to mention the installation of the gage in a curved surface. When the gage is installed so that the outside edge of the probe is flush with the test surface, the center of the gage is then recessed slightly. Given the probe diameter d and the radius of curvature of the model R_c, this amount of recess g is estimated as

$$g = R_c - (R_c^2 - d^2)^{1/2} \sim 0.5R_c\left(\frac{d}{R_c}\right)^2$$

For example, given the present probe diameter d = 3.18 mm on a body with radius 102 mm, the amount of recess is 12 μ, and generally this is negligible compared with the boundary-layer thickness on the body.

TEMPERATURE-RESISTANCE CALIBRATION

The gages were placed in a furnace for a temperature-resistance calibration. The temperature coefficient of resistance α_0 at a reference temperature T_0 is defined by

$$R = R_0[1 + \alpha_0(T - T_0)]$$

where T_0 is normally taken as either 20° or 0°C. A difference in the absolute level of electrical resistance, R_0, among the gages was noticeable despite their physical similarity. The measured temperature coefficient of resistance ranged between 3.72×10^{-3}/°C and 4.17×10^{-3}/°C at 20°C for wires on the six gage specimens tested. The results of the temperature-resistance calibration for the wires in the skin-friction gage used in the cone test described later are shown in figure 2. The difference shown here is close to the extremes at all gages tested. However, as seen later, this did not cause difficulties in actual skin-friction calibration of the gage.

A separate series of tests were conducted to check for potential errors in the temperature-resistance calibration, caused by the expansion of the plastic substrate. While a gage bonded on a plastic substrate alone gave a temperature coefficient of resistance that was considerably higher than that for a free wire, the present configuration, encased within a 3.18-mm-diameter stainless steel tube (fig. 1), gave a value close to that of a free wire. As cited above, there were still differences in temperature coefficients among the gages in casings, and perhaps the variation among the location of electrodes relative to the casing contributed to this difference.

CONDUCTION HEAT LOSSES OF BURIED-WIRE GAGE

The relationship between the heat transfer from this type of gage and the boundary-layer shear stress at the wall has been discussed by other

investigators (refs. 1-3). For present purposes, a correlation in a zero-pressure-gradient, boundary-layer flow may be expressed as

$$\frac{E^2}{R\Delta T} = A(\rho_w \mu_w \tau_w)^{1/3} + B \qquad (1)$$

The left side of equation (1) corresponds to the heat-transfer coefficient of the gage; the quantity B on the right side represents the heat conducted into both the substrate and the fluid medium. Suppose that, with no airflow ($\tau_w = 0$), Fourier's heat conduction law holds and that the material properties remain constant. Then the heat-transfer coefficient, $E^2/R\Delta T = B$, should be a constant, independent of either wire temperature or wall temperature.

However, it is often impossible to maintain a constant wall temperature during the operation of a wind tunnel. For example, in the High Reynolds Number Channel at Ames Research Center (ref. 8), the air temperature falls rapidly over a range of 30°C during blowdown operation and, presumably, the tunnel wall temperature also falls. Thus, it would be of interest to prove whether the above statement on the heat conduction losses of a buried wire gage is factual.

This contention was tested in a series of experimental environments: a single-element, buried-wire gage was placed in a glass bulb and installed in a furnace. The bulb effectively isolated the gage from convection currents produced by a circulation fan within the furnace. In addition, the gage was placed in a vacuum to completely eliminate convection losses. Finally, heat conduction losses were measured on gages within a nonrunning wind tunnel to determine if the laboratory conditions were carried over under conditions when the gages were in use. The conduction heat loss of the gage was then measured by connecting the gage to a constant-temperature, hot-wire anemometer. Both the ambient and wire temperatures were independently varied during the course of the furnace test and, as shown in figure 3, the results indicate that the heat loss depends only on the temperature difference between the wire and the surroundings. The same gage was tested by G. Mateer (private communication, 1978) in the High Reynolds Number Channel and the no-flow heat loss was measured before and after the operation of the tunnel during which large changes in the tunnel wall temperature occur. As a result of the aerodynamic cooling of the tunnel wall (T_{wall} min. was $\sim -12°C$), a larger wire overheat was possible with the same maximum allowable temperature (see below). Mateer's results, also shown in figure 3, are consistent with the results obtained from the furnace test. The slight shift in level between the two tests is considered reasonable because different environments and measuring systems were used. Both test results show a change in the heat-transfer coefficient at low wire overheats. This operating region should obviously be avoided when making skin-friction measurements, particularly when the wall temperature varies. At the higher overheats, the heat-transfer coefficient appears to approach an asymptote, but some variation is still noticeable even at $\Delta T \sim 85°C$. Therefore, when a variation in the wall temperature is encountered during a skin-friction measurement, it is essential that the wall temperature be monitored so that a potential shift in the skin-friction calibration can be taken into account. Even though the highest overheat possible is recommended, the polystyrene material used to construct the present gage sets an

upper bound to the allowable overheat for a given ambient temperature. An excessive wire temperature may loosen the bond between the wire and the substrate and cause erratic measurements.

Note that the heat-loss measurements under no-flow conditions include natural convection losses or conduction into still air, in addition to the conduction of heat into the substrate. Thus, the evaluation of quantity B in the heat-transfer equation by extrapolation of the flowing conditions to zero skin friction may not agree with the no-flow condition. To assess the importance of natural convection effects, additional tests were conducted in the vacuum chamber; these results are also shown in figure 3. The contribution of natural convection to the total heat transfer appears to be significant. In the pilot channel, the measured no-flow heat loss was considerably different from the intercept of the shear stress calibration, as shown in the next section. Generally, it is recommended to evaluate the value of B in equation (1) from extrapolation of the flowing conditions.

In the High Reynolds Number Channel experiment, the measured wall temperature was used in figure 3 to infer the heat conduction loss, and repeatable results were obtained by Mateer over a large temperature variation.

As discussed in the following sections, the calibration of the bidirectional buried wire gage was conducted in the Ames 10- × 15-cm (14 × 6 in.) pilot channel; the experiment on the cone was conducted in the Ames 1.8- × 1.8-m (6- × 6-ft) continuous wind tunnel. The temperature in both tunnels was steady within a few degrees centigrade and no correction on heat conduction loss was needed, but an attempt was made to keep the overheat temperature difference constant with reference to a measured wall temperature. The result was satisfactory.

DIRECTION AND MAGNITUDE CALIBRATION OF SKIN-FRICTION GAGE

The calibration of the gage was conducted in the 10 × 15 cm (4 × 6 in.) Subsonic Wind Tunnel (ref. 9) at Ames Research Center and for which the free-stream Mach number ranged between 0 and 0.6. The skin-friction gage was mounted on a plug that was placed in one of the tunnel walls. The configuration of the plug is shown in figure 4. The probe was rotated about its axis and the probe angle was read from a protractor situated outside the tunnel. A Preston tube and a static pressure port were also placed on the plug and the magnitude of the wall shear stress was deduced using the correlation of Bradshaw and Unsworth (ref. 10), which includes effects of compressibility where applicable. In our test, the gages were operated at 60°C with a DISA 55M10 constant temperature anemometer. The wall temperature was measured by turning off the power to the gage and measuring the cold resistance of the wire between heated wire tests in lieu of a separate wire for temperature monitoring for each data point.

The calibration results for each sensor on the gage placed normal to the flow direction are presented in figure 5. The output from each wire followed the theoretical 1/3 power law, equation (1), quite well.

The directional sensitivity of each sensor is assumed to have the form

$$\frac{E^2}{R\Delta T} = A\ (\rho_w \mu_w \tau_w)^{1/3}\ (\cos^2\alpha + K^2 \sin^2\alpha)^{1/6} + B \tag{2}$$

Here, it is assumed that the conduction heat loss B is independent of flow angle. (Note that equation (2) reduces to a cosine law when the tangential component of skin friction along the sensor is ignored, i.e., $K = 0$.) Then the magnitude and the direction of the skin friction can be determined as follows. Label the two perpendicular buried wires as Nos. 1 and 2, then:

$$\begin{aligned} \frac{E_1^{\,2}}{R_1 \Delta T_1} - B_1 &= A_1 (\rho_w \mu_w \tau_w)^{1/3} (\cos^2\alpha_1 + K_1^{\,2} \sin^2\alpha_1)^{1/6} \\ \frac{E_2^{\,2}}{R_2 \Delta T_2} - B_2 &= A_2 (\rho_w \mu_w \tau_w)^{1/3} (\cos^2\alpha_2 + K_2^{\,2} \sin^2\alpha_2) \end{aligned} \tag{3}$$

If we define

$$S_1 \equiv \left(\frac{E_1^{\,2}}{R_1 \Delta T_1} - B_1 \right) / A_1$$

and (4)

$$S_2 \equiv \left(\frac{E_2^{\,2}}{R_2 \Delta T_2} - B_2 \right) / A_2$$

and if the condition $\alpha_1 + \alpha_2 = \pi/2$ is considered, equations (3) become

$$S_1 = (\rho_w \mu_w \tau_w)^{1/3} (\cos^2\alpha_1 + K_1^{\,2} \sin^2\alpha_1)^{1/6} \tag{5}$$

$$S_2 = (\rho_w \mu_w \tau_w)^{1/3} (\sin^2\alpha_1 + K_2^{\,2} \cos^2\alpha_1)^{1/6} \tag{6}$$

An equation for the wall shear stress is obtained by eliminating α_1 between equations (1) and (2) with the result

$$\rho_w \mu_w \tau_w = \left[\frac{(1 - K_2^{\,2}) S_1^{\,6} + (1 - K_1^{\,2}) S_2^{\,6}}{1 - K_1^{\,2} K_2^{\,2}} \right]^{1/2} \tag{7}$$

As for the direction of the skin-friction vector, equations (5) and (6) show that the quotient of S_1/S_2 is a unique function of the direction, α_1, and is independent of the magnitude of the skin friction. Generally, the two sensors do not have to be perpendicular to one another for this purpose even though it is less convenient to use. McCroskey and Durbin (ref. 5) discussed a measurement of the direction of the shear stress using a film gage; a sensitive form of analyzing the signals suggested by them is

$$\frac{S_1 - S_2}{S_1 + S_2} = f(\theta) = \frac{(\cos^2\alpha_1 + K_1^2\sin^2\alpha_1)^{1/6} - (\sin^2\alpha_1 + K_2^2\cos^2\alpha_1)^{1/6}}{(\cos^2\alpha_1 + K_1^2\sin^2\alpha_1)^{1/6} + (\sin^2\alpha_1 + K_2^2\cos^2\alpha_1)^{1/6}} \tag{8}$$

where θ, the direction of the flow relative to the probe centerline, is equal to $(\pi/4) - \alpha_1$ in the present reference frame.

For unmatched sensors, it may be that $K_1 \neq K_2$, but, as shown below, the difference between the two sensors on each gage tested was found to be small. When it can be assumed that $K_1 = K_2 \equiv K$, then the absolute magnitude of the shear stress in equation (6) takes the simple form:

$$\rho_w \mu_w \tau_w = \frac{(S_1^6 + S_2^6)^{1/2}}{(1 + K^2)^{1/2}} \tag{9}$$

In the calibration of the gage, values of the coefficients of directional sensitivity K_1 and K_2 can be obtained from a plot of $S_1(\alpha_1)$ or $S_2(\alpha_2)$ when these are suitably normalized. The normalizing parameter is the output when one wire sensor is perpendicular to the on-coming shear stress vector.

Figure 6 shows the directional sensitivity of <u>each</u> sensor on the probe at various shear stress levels. The independence of the directional sensitivity on the magnitude of shear stress is demonstrated. Figure 6 also shows the analytical form given in equations (5) and (6) (with a representative value of K_1 and K_2) and demonstrates good agreement with experimental data.

The results of the directional calibration of the buried-wire <u>pair</u> as a bi-directional, skin-friction gage are shown in Figure 7. Experimental data are compared with the analytical form given on the right side of equation (8) with the value $K_1 = K_2 = 0.35$. For practical purposes at small angle of incidence, a visual line fit to the data was used as shown. It is demonstrated that the direction of the skin-friction vector can be determined to within an accuracy of $\pm 5°$, when the flow direction is less than 35°, using the line fit to the data.

The variation of the quantity $(S_1^6 + S_2^6)^{1/2}$ for different yaw angles is shown in figure 8. As suggested by equation (9), the value of this quantity is seen to remain nearly constant over the yaw angle range we surveyed. The magnitude of skin friction obtained with the Preston tube is plotted against the measured values of $(S_1^6 + S_2^6)^{1/2}$ in figure 9. From equation (8), the value of K is determined to be 0.35 for the gage tested, which is consistent with the results in figure 6.

There is an alternative way of obtaining the magnitude of skin friction instead of equation (7) or (9). After determining the direction of the skin friction, one can use equations (1) and (2) to determine the magnitude of the skin friction from the known value of K, but the method introduced above is more direct and convenient to use.

EXPERIMENT ON THREE-DIMENSIONAL SEPARATED TURBULENT FLOW OVER A CONE AT HIGH INCIDENCE

Skin-friction measurements using the bi-directional, buried-wire gages were made on a 1.4-m (54-in.)-long 5° semi-angle circular cone, sting-mounted at 12° angle of attack in the Ames 1.8 × 1.8 m (6- × 6-ft) closed-circuit wind tunnel at M_∞=0.6. Details of the experiment are provided in reference 11.

Figure 10 shows the location of two bi-directional, buried-wire, skin-friction gages on the unwrapped cone surface at the 0.85-length station, and a schematic representation of the lee-side flow field. The same design of Preston tubes, or diameter 0.42 mm (0.016 in.) as used for the gage calibration, was also installed at the 0.85 station to determine the mean level of skin friction at zero incidence, and along the windward generator when the cone was pitched.

Figure 11 provides a comparison between some preliminary surface shear stress directions ω (relative to the cone generators) obtained from oil dot streaks and those angles deduced form the bi-directional, buried hot-wire gage with the cone at an incidence 2.5 times the semi-nose angle. The maximum value of ω given from the gage is close to 40° in the vicinity of the minimum pressure point near $\phi \sim 100°$. (Note that the circumferential angle ϕ is measured from the windward to the leeward generator.) The boundary layer, in proceeding around the lee-side of the cone, encounters a strong circumferential adverse pressure gradient and thickens rapidly. The cross-flow angle ω reduces progressively to zero, at which point the shear stress trajectories converge and run parallel to a generator, the primary separation line, ϕ_{s1} (see schematic drawing in fig. 10). The second pressure minimum, caused by the induced effect of the primary vortices, drains fluid from the region of the leeward generator, appreciably thinning the flow there. This movement of fluid beneath the vortices itself separates from the cone surface at ϕ_{s2}, on a scale substantially smaller than the primary flow. Between ϕ_{s1} and ϕ_{s2}, there must be yet another divergent attachment line region where $\omega = 0$ (see figs. 10 and 11), from which fluid diverges to feed both separation lines at ϕ_A.

The qualitative agreement between the oil-flow results and the buried-wire results is satisfactory, but figure 11 reveals a discrepancy in magnitude of the shear stress angle. The explanation for the discrepancy will be pursued in a forthcoming repeat experiment.

The variation in magnitude of the resultant surface shear stress at the 0.85-axial station in subsonic flow obtained from a bi-directional, buried-wire gage is shown in figure 12 (note that the Preston tube "fixes" the level at one point). The maximum uncertainty in the absolute levels of shear stress deducible from the buried-wire gages is about ±15%. The variation of the local skin-friction coefficient with circumferential angle at Mach 0.6 follows the trends established in Rainbird's (ref. 12) Mach 1.8 and 4.25 measurements. The skin friction reduces smoothly to a minimum, but finite, value at the primary separation line that is lower than the zero incidence value for attached flow. The skin friction is again minimum at the secondary separation, with high values due to the divergent attachment line flows between the separation lines and along the leeward meridian. In fact, the boundary layer along the leeward generator accelerates rapidly in the lateral sense due to the very favorable pressure gradient caused by the primary vortices. The shear stress increases to a value well above that at the windward generator with a concomitant surface shear direction of -20° at $\phi \sim 170°$.

CONCLUSIONS

The fabrication, calibration, and testing of a new type of skin-friction gage consisting essentially of a pair of buried (yawed) hot wires on a polystyrene substrate, has been performed. Sample gages were then mounted in the surface of a circular cone, which measured the magnitude and direction of the shear stress beneath the three-dimensional separated turbulent boundary layers at Mach 0.6. A point calibration was also provided by the Preston tube. The device shows good potential for general use with three-dimensional boundary layers in both subsonic and supersonic flows, but very careful calibration and monitoring of the conduction heat loss must be made frequently to offset the problems with drifting of the signal levels.

REFERENCES

1. Ludwieg, H.: Instrument for Measuring the Wall Shearing Stress of Turbulent Boundary Layers. NACA TM 1284, 1950.

2. Liepmann, H. W.; and Skinner, G. T.: Shearing-Stress Measurements by Use of a Heated Element. NACA TN 3268, 1954.

3. Brown, G. L.: Theory and Application of Heated Films for Skin Friction Measurements, Proceedings of the 1967 Heat Transfer and Fluid Mechanics Institute, Stanford University Press, Stanford University, Calif., pp. 369-381.

4. Drinkuth, R. H.; and Pierce, F. J.: Directional Heat Meter for Wall Shear Stress Measurements in Turbulent Boundary Layers. The Review of Scientific Instruments, vol. 37, no. 6, June 1966, pp. 740-741.

5. McCroskey, W. J.; and Durbin, F. J.: Flow Angle and Shear Stress Measurements Using Heated Films and Wires. ASME Journal of Basic Engineering, vol. 94D, 1972, pp. 46-52.

6. Rubesin, M. W.; Okuno, A. F.; Mateer, G. G.; and Brosh, A.: A Hot-Wire Surface Gage for Skin Friction and Separation Detection Measurements. NASA TM X-62,465, 1975.

7. Murthy, V. S.; and Rose, W. C.: Buried Wire Gage for Wall Shear Stress Measurements. AIAA Paper 78-798, 1978.

8. Mateer, G. G.; Brosh, A.; and Viegas, J. R.: A Normal Shock-Wave Turbulent Boundary-Layer Interaction at Transonic Speeds. AIAA Paper 76-161, 1976.

9. Sandborn, V. A.; and Seegmiller, H. L.: Evaluation of Mean and Turbulent Velocity Measurements in Subsonic Accelerated Boundary Layers. NASA TM X-62,488, March 1976.

10. Bradshaw, P.; and Unsworth, K.: A Note on Preston Tube Calibrations in Compressible Flow. Imperial College Aero Rept. 73-07, 1973.

11. Peake, D. J.; Owen, F. K.; and Higuchi, H.: Symmetrical and Asymmetrical Separation About a Yawed Cone. AGARD CP-247, October 1978.

12. Rainbird, W. J.: The External Flow Field About Yawed Circular Cones. AGARD CP-30, May 1968.

ORIGINAL PAGE IS
OF POOR QUALITY

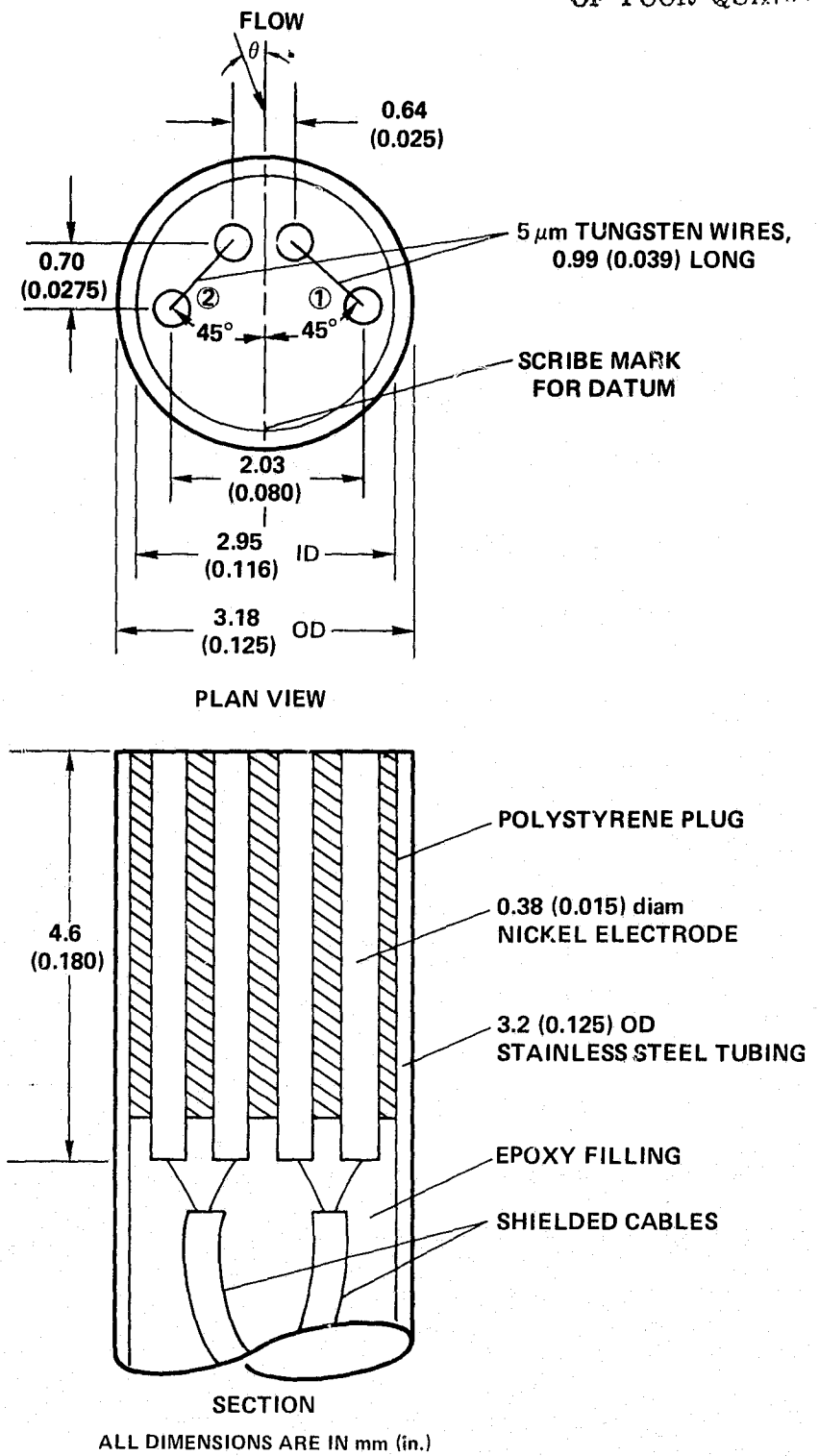

Figure 1.- Drawing of bi-directional, buried-wire, skin-friction gage.

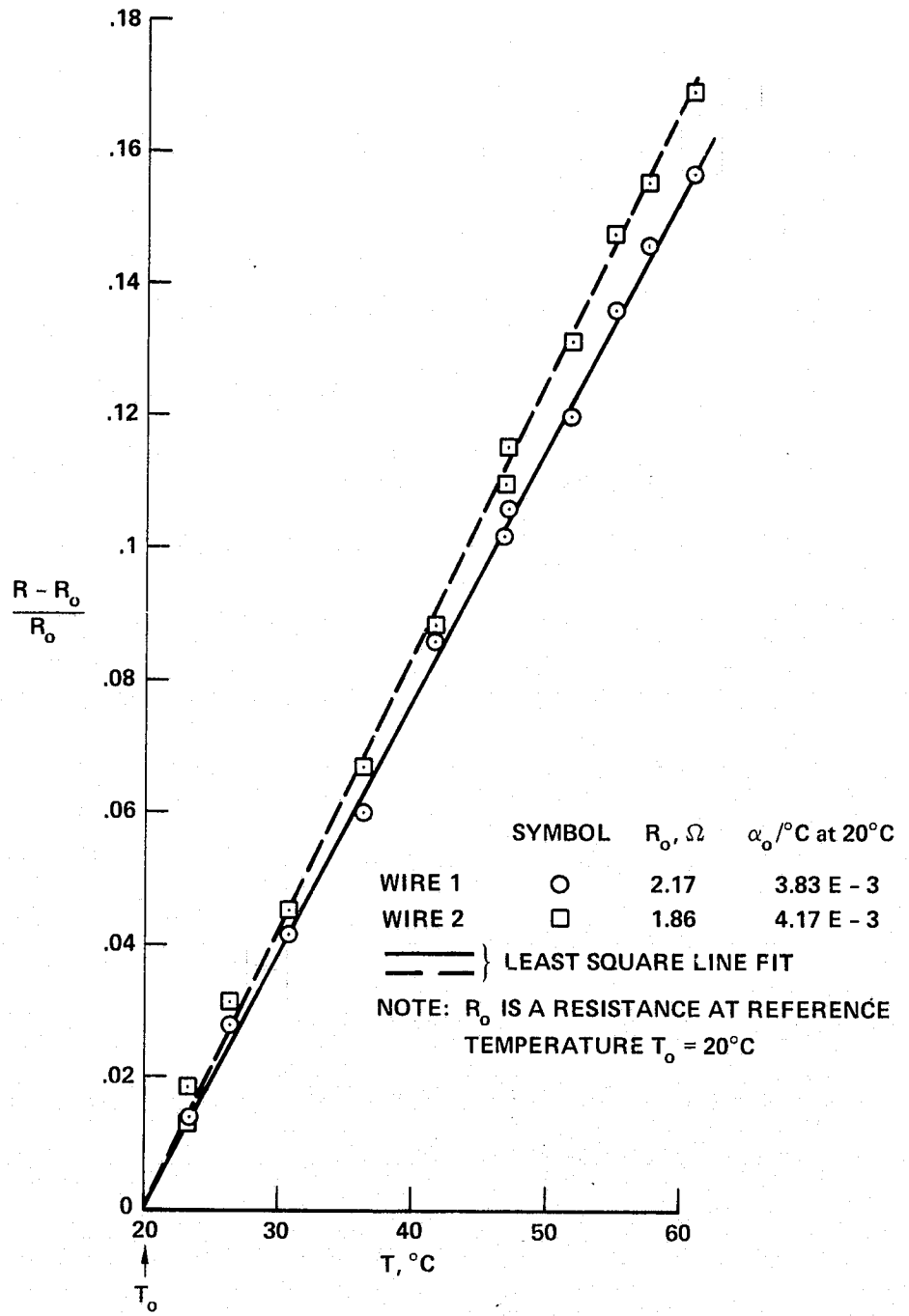

Figure 2.- Temperature-resistance calibration.

ORIGINAL PAGE IS
OF POOR QUALITY

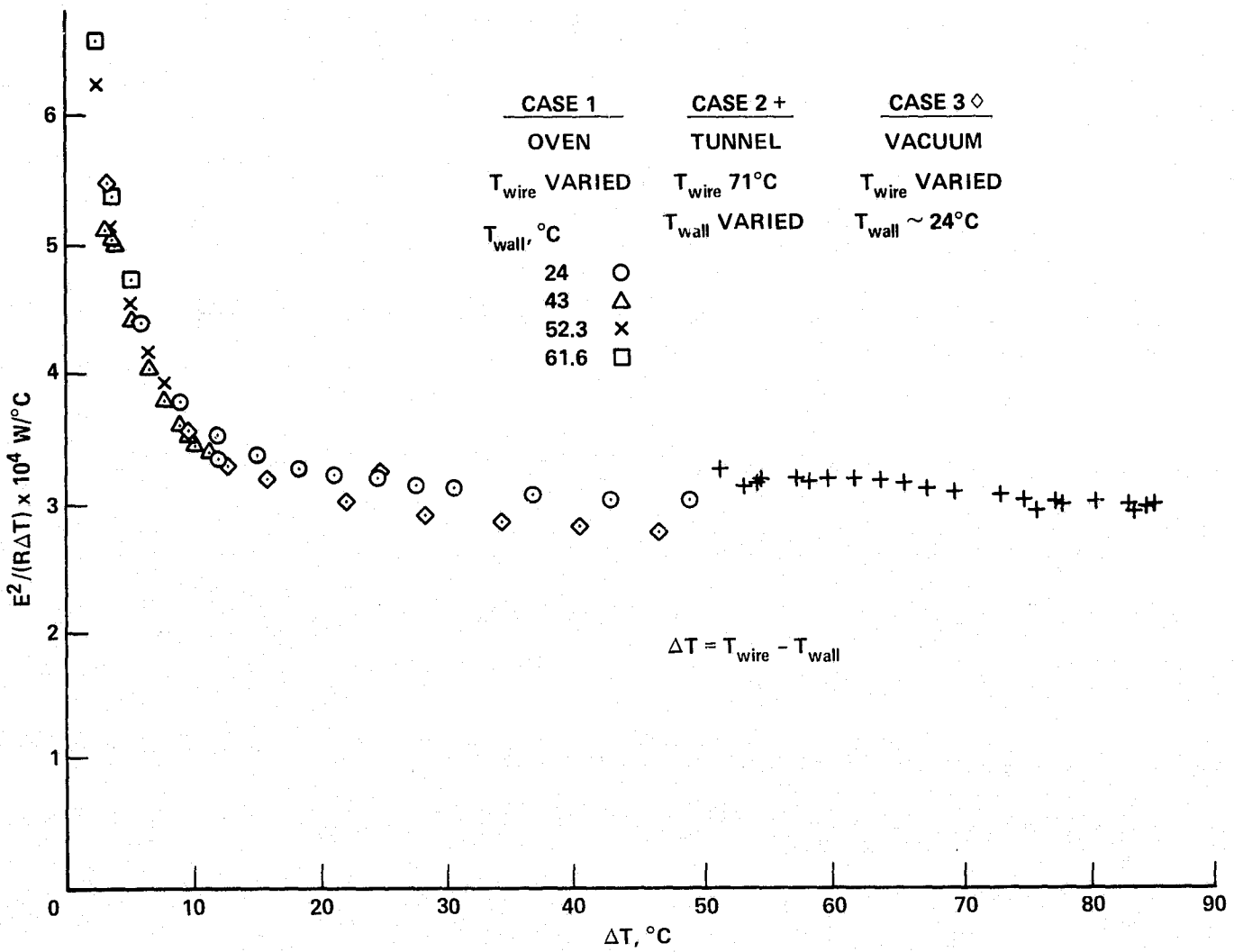

Figure 3.- Conductive heat-transfer measurements for the single-element, buried-wire, skin-friction gage, with 5-μ-diameter, 1.59-mm-long tungsten wire.

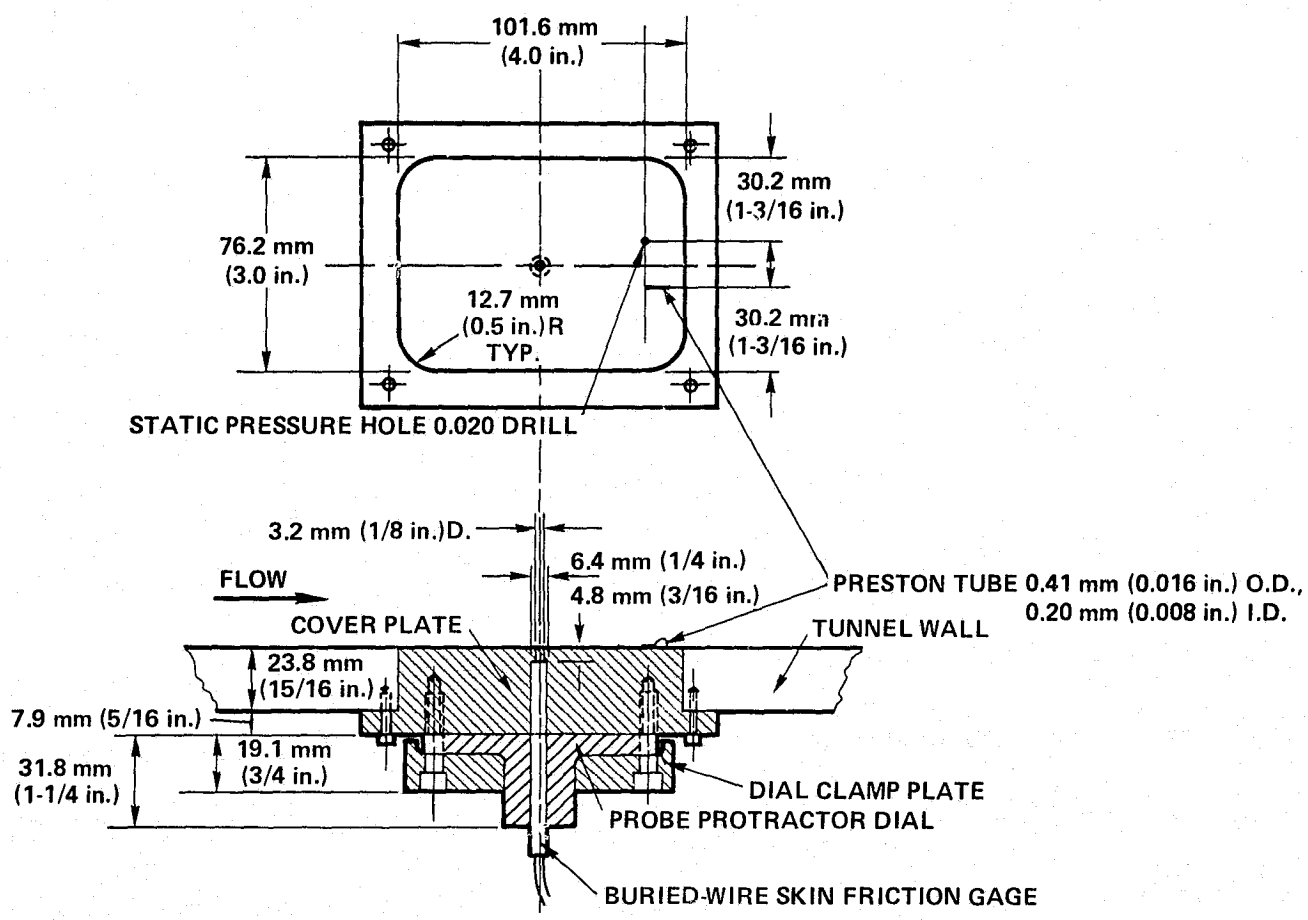

Figure 4.- Skin-friction gage calibration plug.

ORIGINAL PAGE IS
OF POOR QUALITY

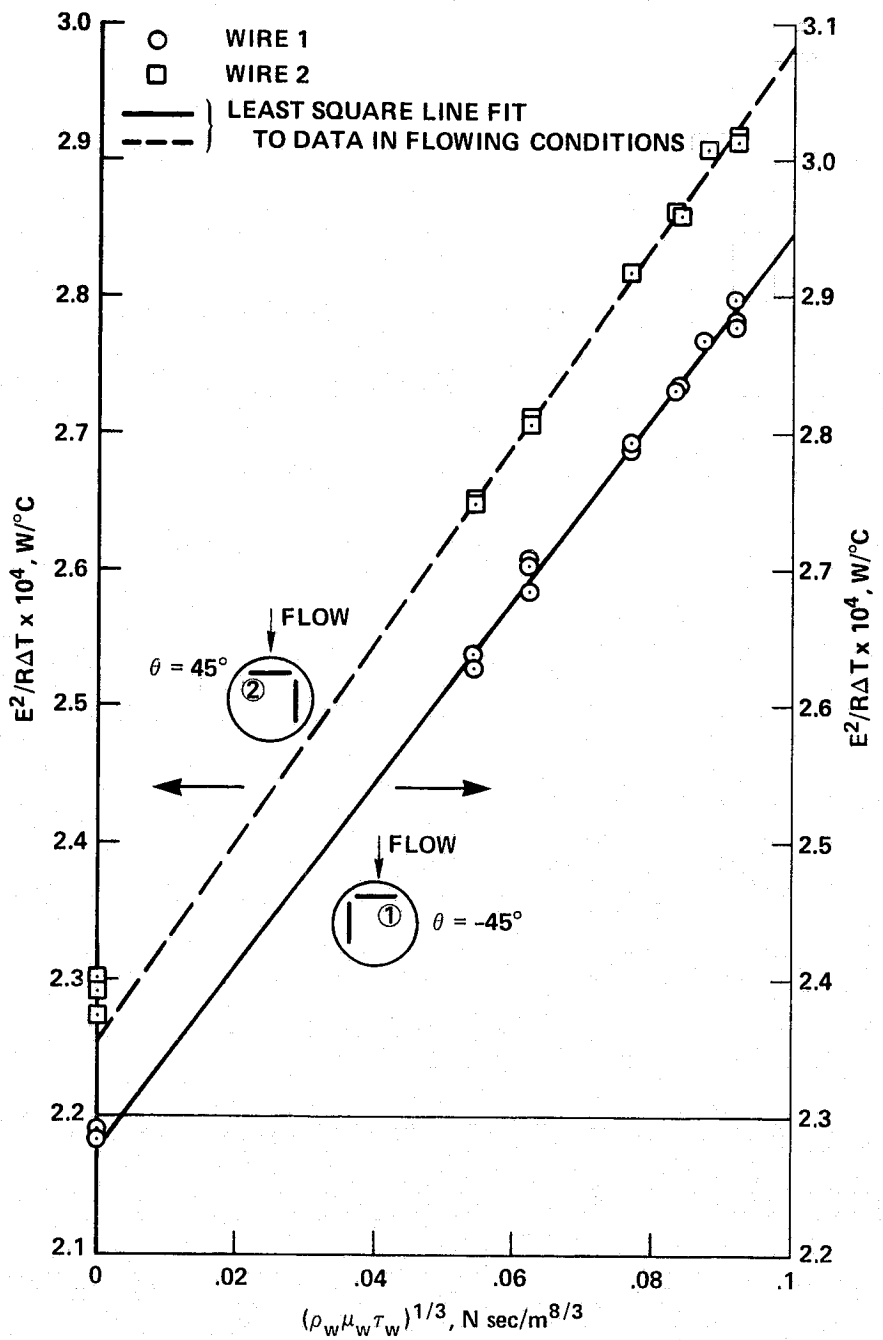

Figure 5.- Calibration of each element of bi-directional, buried-wire gage normal to flow.

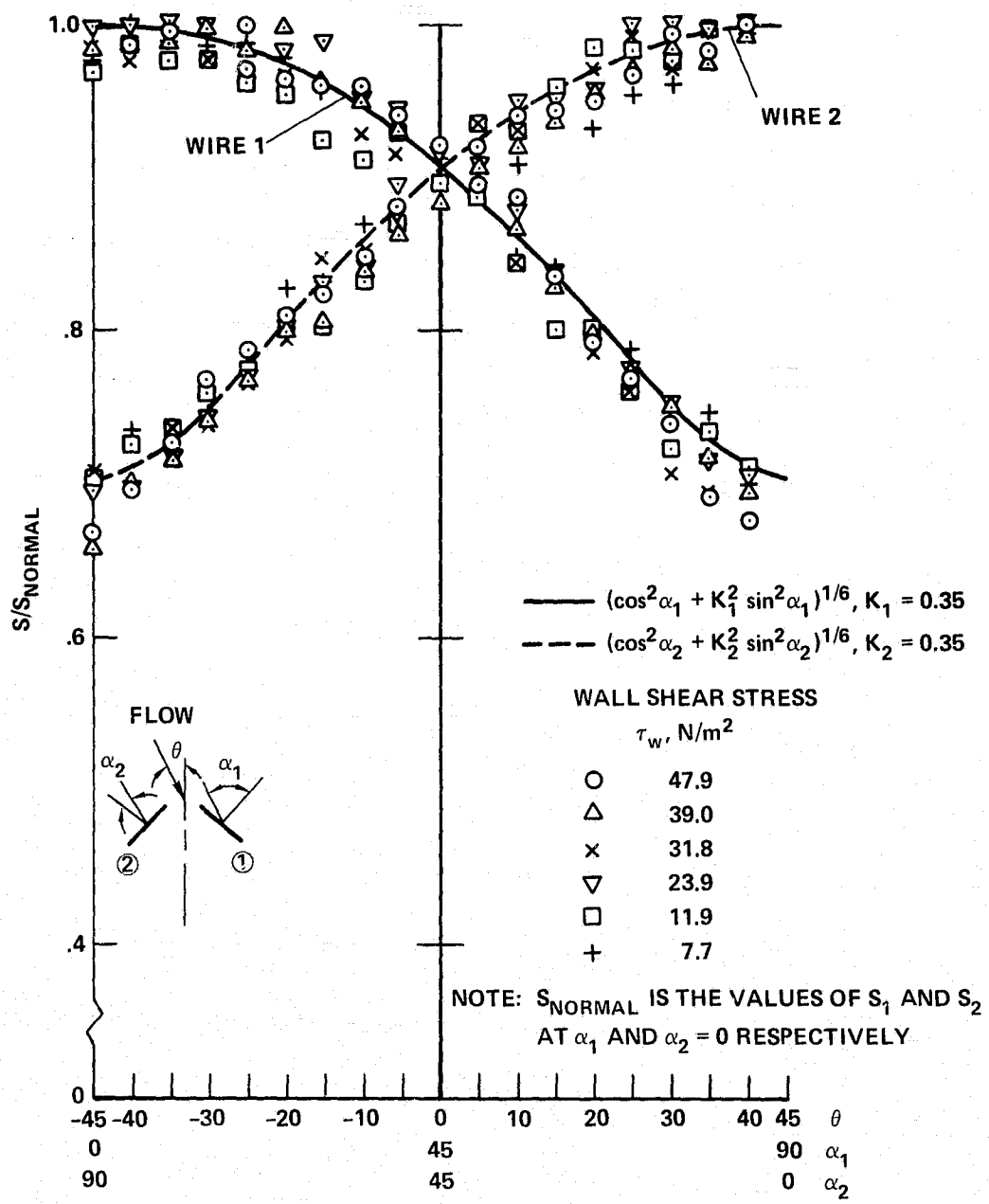

Figure 6.- Directional sensitivity of each element of bi-directional, buried-wire gage.

ORIGINAL PAGE IS
OF POOR QUALITY

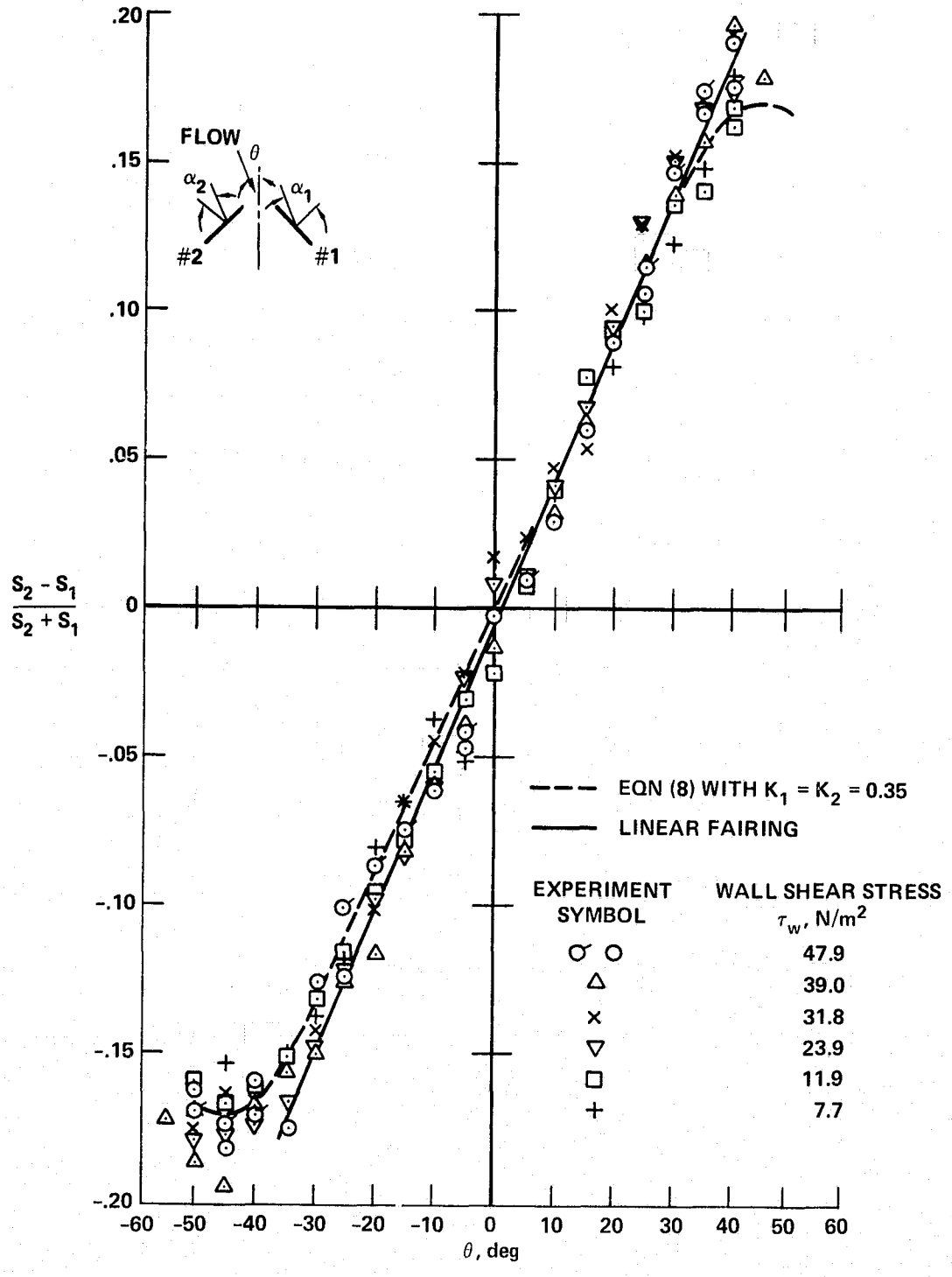

Figure 7.- Directional calibration of bi-directional, buried-wire gage.

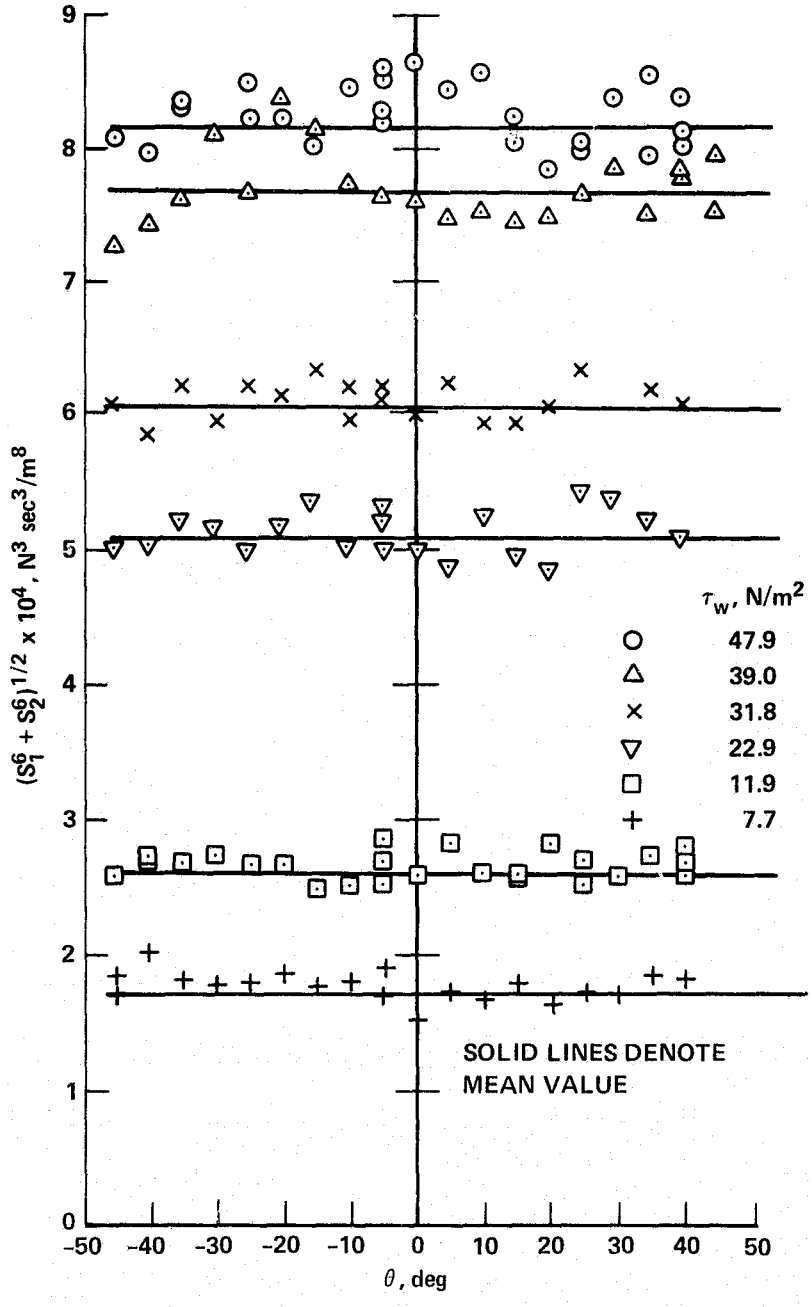

Figure 8.- Magnitude sensitivity of bi-directional, buried-wire gage.

ORIGINAL PAGE IS
OF POOR QUALITY

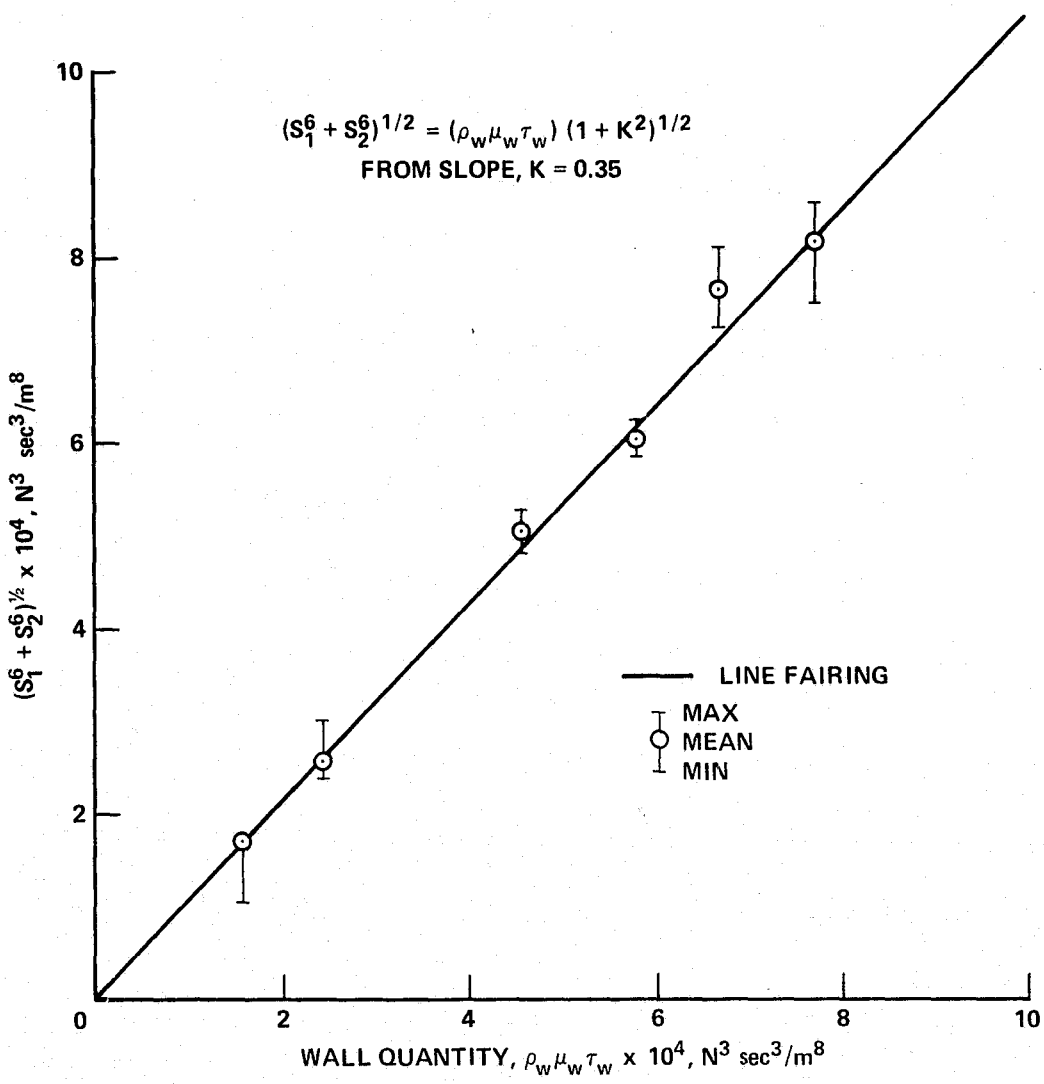

Figure 9.- Magnitude calibration of bi-directional, buried-wire gage.

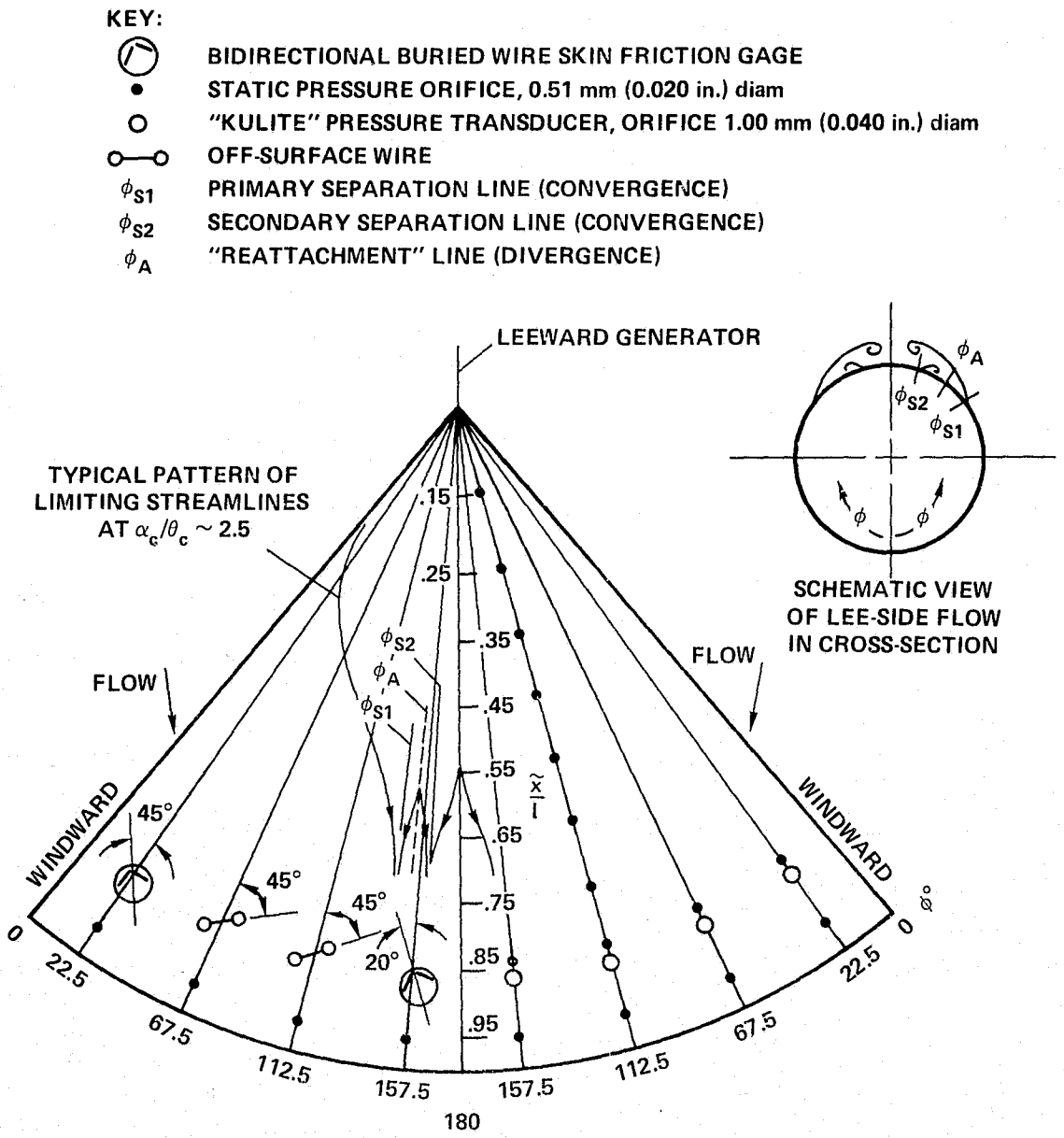

Figure 10.- Instrumentation on unwrapped cone surface and schematics of lee-side flow in cross section.

ORIGINAL PAGE IS
OF POOR QUALITY

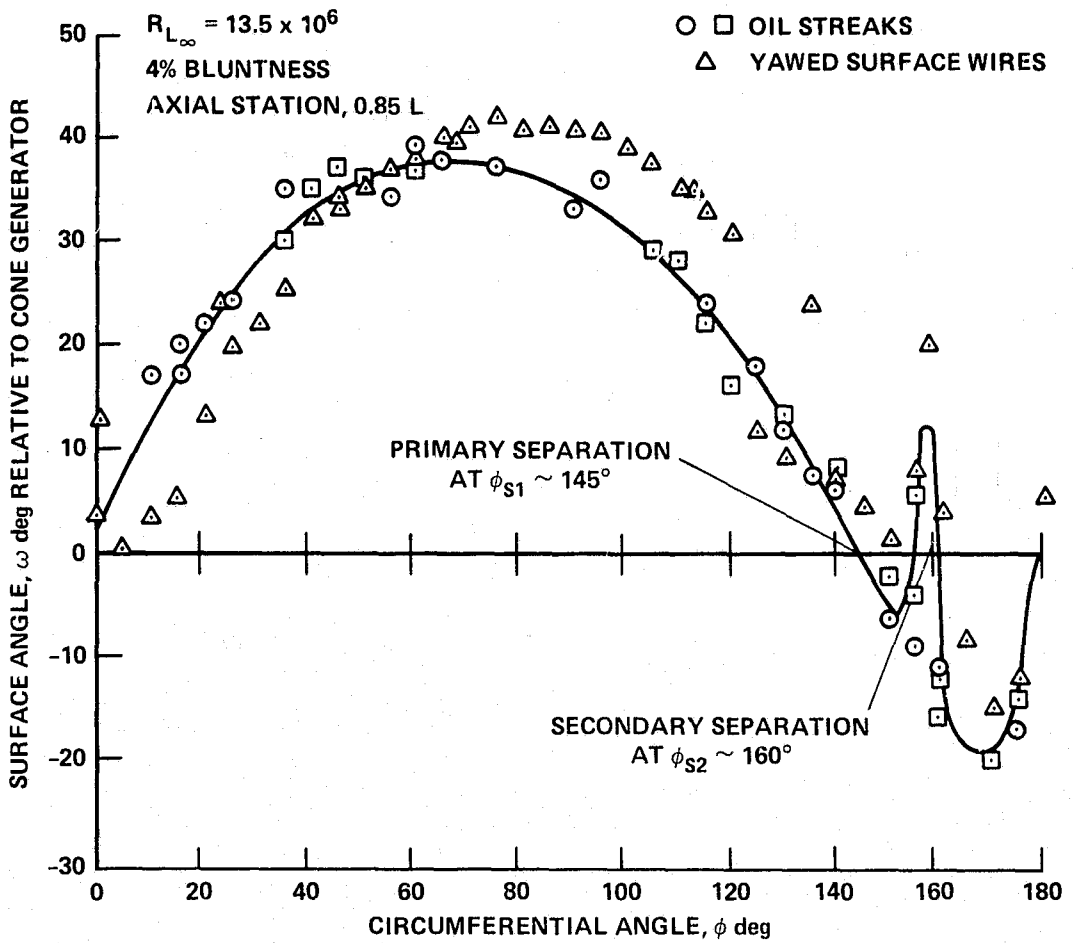

Figure 11.- Wall shear stress directions, M_∞ = 0.6, α_c/θ_c = 2.5.

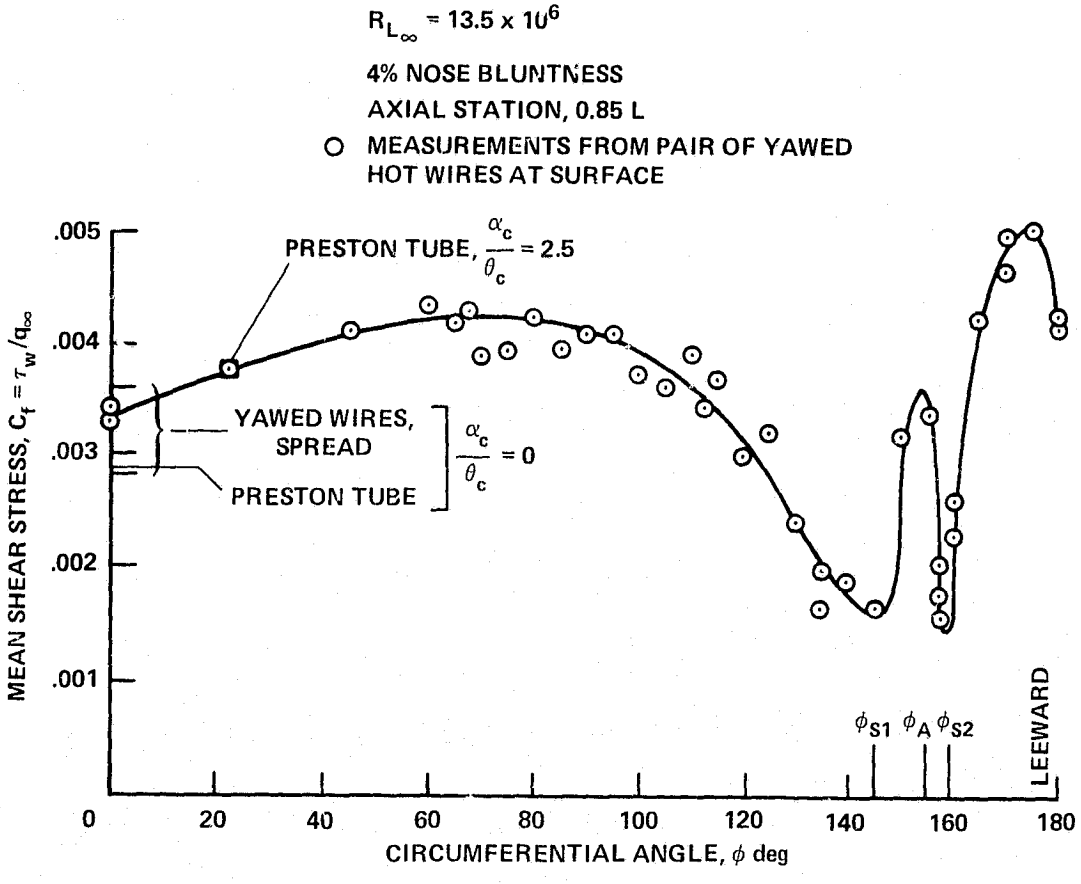

Figure 12.- Wall shear stress magnitude, $M_\infty = 0.6$, $\alpha_c/\theta_c = 2.5$.